On direct internal methane steam reforming kinetics in operating solid oxide fuel cells with nickel-ceria anodes

Thallam Thattai, A.; van Biert, Lindert; Aravind, P. V.

DOI
10.1016/j.jpowsour.2017.09.082

Publication date
2017

Document Version
Final published version

Published in
Journal of Power Sources

Journal of Power Sources 370 (2017) 71–86

Contents lists available at ScienceDirect

Journal of Power Sources

journal homepage: www.elsevier.com/locate/jpowsour

On direct internal methane steam reforming kinetics in operating solid oxide fuel cells with nickel-ceria anodes

A. Thallam Thattai*, L. van Biert, P.V. Aravind

Process & Energy Laboratory, Delft University of Technology, Leeghwaterstraat 39, 2628CB Delft, The Netherlands

HIGHLIGHTS

- Experimental study on MSR global kinetics in SOFCs with low steam to carbon ratios.
- Significant differences in characteristic profiles for different kinetic approaches.
- Importance of studying global and elementary MSR kinetics on ceria anodes.
- Effect and importance of metallic current collector (mesh) on fuel reforming.

ARTICLE INFO

Article history:
Received 2 June 2017
Received in revised form
8 September 2017
Accepted 28 September 2017
Available online 14 October 2017

Keywords:
Solid oxide fuel cells
Methane steam reforming
Kinetics
Experimental
Langmuir-Hinshelwood
Power law

ABSTRACT

Major operating challenges remain to safely operate methane fuelled solid oxide fuel cells due to undesirable temperature gradients across the porous anode and carbon deposition. This article presents an experimental study on methane steam reforming (MSR) global kinetics for single operating SOFCs with Ni-GDC (gadolinium doped ceria) anodes for low steam to carbon (S/C) ratios and moderate current densities. The study points out the hitherto insufficient research on MSR global and intrinsic kinetics for operating SOFCs with complete Ni-ceria anodes. Further, it emphasizes the need to develop readily applicable global kinetic models as a subsequent step from previously reported state-of-art and complex intrinsic models. Two rate expressions of the Power law (PL) and Langmuir-Hinshelwood (LH) type have been compared and based on the analysis, limitations of using previously proposed rate expressions for Ni catalytic beds to study MSR kinetics for complete cermet anodes have been identified. Firstly, it has been shown that methane reforming on metallic (Ni) current collectors may not be always negligible, contrary to literature reports. Both PL and LH kinetic models predict significantly different local MSR reaction rate and species partial pressure distributions along the normalized reactor length, indicating a strong need for further experimental verifications.

1. Introduction

Significant changes in global energy markets make it necessary to develop decentralised, novel, efficient and flexible energy technologies. Among conventional fossil fuels, natural gas is considered relatively cleaner (lower carbon footprint and emissions) [1], and thus research into the development of novel gas based technologies is important to ensure clean and efficient power production. Fuel cells offer many advantages compared to conventional gas/steam turbine based electricity production in terms of efficiency and flexibility [2]. Fuel flexible, high temperature solid oxide fuel cells (SOFCs) are capable of internally converting hydrocarbon fuels like natural gas (methane), syngas into electricity and heat with high electrical efficiencies upto 60% [3] and low CO_2, NO_x, SO_x emissions.

Internal methane reforming in SOFCs can be carried out either using mainly steam (methane steam reforming or MSR (Eqn. (1)) and/or CO_2 (dry reforming) as a reforming agent. Steam is still the most commonly used reforming agent, although the use of CO_2 is also being much researched upon in the recent past focussing on biogas as a fuel [4–6]. The endothermic MSR reaction produces syngas, a mix of CO and H_2 as shown in Eqn. (1). The produced CO could also react with steam at high temperature via the water gas shift (WGS) reaction (Eqn. (2)) to produce CO_2 and H_2. The WGS reaction is generally assumed at/near equilibrium; the reaction being much faster than the MSR reaction [7–9].

* Corresponding author.
E-mail address: A.ThallamThattai@tudelft.nl (A. Thallam Thattai).

https://doi.org/10.1016/j.jpowsour.2017.09.082

$$CH_4 + H_2O \rightleftharpoons CO + 3H_2 \qquad \Delta H^0_{298} = 205.8\text{KJ mol}^{-1} \tag{1}$$

$$CO + H_2O \rightleftharpoons CO_2 + H_2 \qquad \Delta H^0_{298} = -41\text{KJ mol}^{-1} \tag{2}$$

The possibility of direct internal methane reforming in SOFCs offers many advantages like high conversion efficiency, allows to overcome the need of an external reformer, reduce heat transfer and blower losses, cost and complexity. A fully integrated SOFC unit also helps to avoid extensive fuel preparation facilities. However, despite these advantages there exist multiple challenges to safely and continuously operate direct internal methane reforming SOFCs. Major issues arise due to difference in reaction rates, location of occurence and thermodynamic behaviour between the MSR reaction and the electrochemical oxidation reactions (Eqn. (3)). The electrochemical reaction(s) is responsible for the flow of electrons and ions thereby producing current, steam, power and heat. The interaction between the slower MSR reaction and exothermic H_2 electrochemical oxidation is complex and not well understood.

$$\begin{aligned} H_2 + O^{-2} &\rightarrow H_2O + 2e^- \\ 0.5O_2 + 2e^- &\rightarrow O^{-2} \end{aligned} \tag{3}$$

Nickel (Ni) based anodes have been used widely in SOFCs, as Ni is a well known methane reforming catalyst [10]. Due to the large number of catalytic (Ni) sites available in the porous anode, the MSR reaction is relatively fast [11]. In addition to H_2, CO could also undergo direct electrochemical oxidation, however H_2 oxidation is reported to be more preferential, particularly on Ni and ceria based anodes [12]. The MSR reaction is endothermic, while the WGS reaction is slightly exothermic. This in combination with different reaction rates leads to undesirable temperature gradients in the anode. However, the heat released by the electrochemical reactions in the SOFC helps promote the MSR reaction. The main focus towards ensuring safe and long term SOFC operation with internal MSR would be reduce these undesirable temperature gradients in the cell/stack. Furthermore, the presence of Ni in the hydrocarbon fuelled SOFC anode also promotes carbon formation and deposition, which causes rapid cell degradation.

An important step to reduce these temperature gradients and carbon deposition within methane(or natural gas) fuelled SOFC anodes is to improve our understanding on MSR reaction kinetics, both under open circuit conditions and in operating mode i,e under the influence of current. Sophisticated and intrinsic micro kinetic models have been developed in the past [13,14] to accurately predict species, temperature and electrochemical parametric distribution across the anodes using elaborate heterogeneous reaction mechanisms. However, MSR global reaction kinetics on Ni catalysts has also been extensively studied experimentally in the past decades by numerous researchers, particularly using test catalytic reactors and catalyst beds [4,15–20]. Since the last decade, experimental research has also been carried out on MSR global kinetics in Ni based SOFC anodes. A comprehensive review on these studies can be found in multiple review articles [1,19,21]. Internal MSR global kinetic studies on SOFCs in literature can be broadly classified in 3 categories, based on the type of reaction rate expression used: power law (PL) expressions, first order (FO) in methane and Langmuir-Hinshelwood (LH) type expressions [11]. The three approaches differ significantly with respect to the their assumptions, making the choice for a rate expression challenging. The PL approach simplifies the analysis a lot by ignoring the reaction mechanism and elementary steps while with LH expressions, care has to be taken in formulating the rate expression using appropriate adsorption/desorption parameters. The FO kinetic models can be considered as a subset of the general LH kinetic models with dissociative adsorption of methane as the only rate determining step, resulting in a reaction rate dependence only on the partial pressure of methane.

There are often large overlaps in the use of MSR reaction rate expressions among industrial catalyst studies and cermet SOFC anode studies. However an important aspect to keep in mind is that, with a cermet anode, the ceramic is generally an oxygen-ion conductor while with industrial catalysts the support material (e.g, alumina) is not. Additionally the porous structure in a cermet anode is not the same as in a catalyst bed. There has been no study in literature which brings out the limitations of using MSR rate expressions for SOFC cermet anodes, previously developed for industrial Ni catalysts. In order to improve and fully understand SOFC performance with internal MSR, researchers have to carry out extensive experimentation with complete SOFC cermets/cells/stacks not only in open circuit conditions but also under the influence of current.

Table 1 shows a summary of the relevant internal MSR kinetic studies (experimental) reported in literature using Ni based SOFC cermet anodes. The assumed reaction rate expression and its type has been listed with important operating parameters like the cell temperature, steam to carbon ratio and current density. The table clearly shows that the reported kinetic parameters (activation energy E_a, pre-exponenetial factor (k), reaction orders) differ significantly and thus it is very challenging to attain consensus. It is not appropriate to compare the results on a quantitative basis from these studies, as they have been carried out in a varied set of operating conditions, test benches and cell geometries. Furthermore, the approach for experimental data management and analysis (for eg, fitting of parameters, error estimation etc.) also varies widely.

The table further shows the lack in experimental efforts on MSR kinetics with operating SOFCs i,e under the influence of current. Despite the additional complexity introduced due to current, it is important to obtain experimental data and establish kinetic trends for the MSR reaction in operating SOFCs. Majority experimental investigations on internal MSR on SOFCs have been carried out with high steam to carbon.

(S/C) ratios (>1.5), mostly for safe operation and to prevent carbon deposition. Steam is an expensive commodity in industry and in order to reduce steam consumption while operating Ni based SOFCs with methane as fuel, it is important to conduct experiments with lower S/C ratios. Only a few research groups have conducted tests with relatively low S/C ratios (<1.5) as seen from Table 1.

Another important aspect not clearly reported by experimental studies in literature is the effect of the metallic current collector (mesh) itself on methane reforming. Studies on MSR kinetics using SOFC cermet anodes (Table 1) in literature often do not investigate the influence of the current collector (mesh) itself on reforming, assuming it to be negligible and without providing adequate justification. The mesh used is usually metallic (like Ni/Pt) which, as aforementioned, is a good reforming catalyst. No study has been found in literature which tries to adequately quantify the extent of reforming on the Ni/Pt mesh. In the investigation reported by Souentie et al. [26], the authors have mentioned an insignificant catalytic rate on the Ni mesh, however no clear quantification has been reported.

A suitable combination of the SOFC anode material and operating conditions can ensure safe methane fuelled operation without significant carbon formation. Ceria has been of much interest as an anode material due to its high electrocatalytic activity without additives and its higher resistance to carbon deposition compared to the conventional YSZ material [12,32–35]. The polarisation resistance for H_2 oxidation on ceria is shown to be

Table 1
Literature summary on MSR reaction kinetics with Ni based cermet anodes.

Reference	Material/ configuration	Type of kinetic rate expression	Rate expression	Temperature range °C	S/C ratio	Current density ($A(m^2)^{-1}$)	Kinetic parameters
Nakagawa et al. [22]	Ni-YSZ-CeO2 anode	LH	$r_{CH_4} = \frac{K1.K2.K3.p_{CH_4}.p_{H_2O}}{(1+K2.p_{CH_4}+K3.p_{H_2O})^2}$	700–1000	2–8	6000	$E_a = 18$ kJ mol^{-1}
Achenbach et al. [23]	Ni-ZrO2 cermet	FO	$r_{CH_4} = k_0.\exp(-E_a/RT)\left(1-\frac{p_{CO}.p_{H_2}^3}{p_{CH_4}.p_{H_2O}.K_p}\right)p_{CH_4}$	700–940	2.6–8	–	$k_0 = 4274$ mol (s-m^2-bar)$^{-1}$ $E_a = 82$ kJ mol^{-1}
Parsons et al. [24]	Ni cermet	PL	$r_{CH_4} = k.(p_{CH_4})^{1.25}$	960	3	–	$k = 2.4$ e−3 mol.s^{-1}.atm$^{-1.25}$
Lee et al. [25]	Ni-YSZ cermet	FO	$r_{CH_4} = k_0.\exp(-E_a/RT).p_{CH_4}(p_{H_2O})^{\alpha}$	800–1000	2–7.4	–	$E_a = 98.23$ kJ mol^{-1} $\alpha = -1.25$
Souentie et al. [26]	Ni-GDC and Au-Ni-GDC anode	LH	$r_{CH_4} = \frac{k_a.p_{CH_4}}{1+k.\left(\frac{p_{CH_4}}{p_{H_2O}}\right)}$	800–900	0.25,1	2500	$E_a = 96$–117 kJ mol^{-1} $k_a = 15$-45e-06, $k = 0.23$
Dicks et al. [27]	Ni-YSZ anode	LH	$r_{CH_4} = \frac{k.p_{CH_4}}{\left(1+K_H.p_{H_2}^{0.5}+K_S.\frac{p_{H_2O}}{p_{H_2}}\right)^2}$	700–1000	1–7	–	$E_a = 135$ kJ mol^{-1} $k_0 = 21$ mol (s-cm^2-bar)$^{-1}$
Belyaev et al. [28]	Ni-ZrO2-CeO2 electrode	FO	$r_{CH_4} = k.p_{CH_4}$	800–850	2–4	147	$E_a = 163$ kJ mol^{-1}
Bebelis et al. [29]	Ni-YSZ cermet film	LH	$r_{CH_4} = k_{ad}.p_{CH_4}.\left(1-\frac{k_{ad}}{k_r.K_{H_2O}}.\frac{p_{H_2}.p_{CH_4}}{p_{H_2O}}\right)$	800–900	0.2 –10	–	$E_a = 230$ kJ mol^{-1}
Ahmed et al. [30]	Ni-YSZ anode	PL	$r_{CH_4} = k_0.\exp(-E_a/RT).p_{CH_4}^{\alpha}.p_{H_2O}^{\beta}$	854–907	1.4 –3.0	–	$\alpha = 0.85$, $\beta = -0.35$ $E_a = 95$ kJ mol^{-1}
Timmermann et al. [31]	Ni-CGO and Ni-YSZ anodes	PL	$r_{CH_4} = k_0.\exp(-E_a/RT).p_{CH_4}^{n}.p_{H_2O}^{m}$	800,950	0–3	–	$k_0 = 4.05$e-05 mol (s-m^2-Pa$^{1.19}$)$^{-1}$ $E_a = 26.3$ kJ mol^{-1}, $m = 0$, $n = 1.19$
Fan et al. [7]	Ni-GDC anode	PL	$r_{CH_4} = k_0.\exp(-E_a/RT).p_{CH_4}^{\alpha_{CH_4}}.p_{H_2O}^{\alpha_{H_2O}}$	700–750	1.5 –2.45	1000	$E_a = 63$–88 kJ mol^{-1} $\alpha_{CH_4} = 0.7$, $\alpha_{H2O} = -0.08$

lower than purely Ni based anodes [36]. Furthermore, MSR activation energies with ceria doped anodes are also reported to be lower than Ni-YSZ anodes [23,29]. Gadolinium doped ceria (GDC) has been of much interest since the recent past as a SOFC anode material due to its improved performance with direct utilization of methane [32,35,37–39]. Ni-GDC cermet anodes have been used to investigate reforming kinetics in the past [7,26,40] particularly due to their high electrocatalytic activity, resistance to carbon deposition and relatively higher contaminant (like H_2S/HCl) tolerance.

MSR global kinetic studies comparing Ni-YSZ anodes with ceria based anodes have been carried out previously [31] and it has been shown that ceria plays an important role in methane conversion and charge transfer chemistry. However, there have yet been no major efforts on carrying out global and intrinsic kinetic studies on Ni-ceria based anodes with low S/C ratios.

The lack in experimental investigations on internal MSR in operating SOFCs also adversely affects modeling research. SOFC models are helpful tools as they allow us to predict temperature profiles/gradients within the cell/stack and thereby develop optimal operating conditions. Since the last few years, extensive modeling efforts have been taken by multiple research groups towards modeling SOFCs with internal MSR. Many types of models (CFD, steady/dynamic state sytems, cell/stack design concepts, micro-models) have been developed and reported in literature, an elaborate review on which can be found in many articles [1,11,19,41–45]. Sophisticated and state of the art intrinsic models developed for Ni-YSZ anodes and high (around 3–4) inlet S/C ratios [13,14] are extremely helpful in fundamental understanding and in obtaining accurate local sensitivity of various parameters to cell performance. However, such models need an extensive and validated heterogeneous multi-step reaction mechanism to solve the coupled set of transport equations. Additionally, solving the coupled set of equations is a very challenging task due to the large number of involved species, complexity to incorporate effects of distributed electronic/ionic potentials and the numerical stiffness of the equation set.

SOFC system developers and manufacturers rely largely on dynamic models (both system level and CFD) for operation and control, wherein, implementation of such elaborate reaction mechanisms is extremely complex [46] and computationally expensive. Many research groups have developed dynamic SOFC cell/stack/system level models wherein MSR kinetics is accounted for using first order (FO) or LH rate expressions [47–50]. However, adequate justification on the use of these rate equations in dynamic models is never reported. The authors agree that based on rigorous micro-model analysis, appropriate rate determining steps could be determined to develop more applicable global kinetic models and subsequently be used to develop reliable dynamic models.

A recent article by Ahmed et al. [51] has further pointed out the effects of using two rate expressions (of PL and FO type) on operating parameters like current density, temperature and cell voltage using a 1-D model. Development of reliable SOFC models requires reliable experimental data in terms of kinetic parameters. Reaction rate expressions using one of the 3 aforementioned approaches (PL/FO/LH) are fitted for the experimentally obtained methane conversion data with appropriate optimization scripts/subroutines to obtain various kinetic parameters. Despite significant progress in the conceptual formulation of MSR reaction rate expressions using these approaches, there exists a shortage in experimental efforts with Ni-ceria anode based operating SOFCs. Additionally a comparison between the kinetic approaches using experimental data has never been reported.

In a nutshell, this article highlights the importance of carrying out experimental internal MSR global and intrinsic kinetic studies with complete Ni-ceria cermet anodes under the influence of current and further brings forward some limitations of using previously proposed rate equations to study global MSR kinetics on complete cermet anodes. A step by step experimental approach to study global MSR kinetics is presented with a focus on low inlet S/C ratios (around 1) and moderate current densities (I_c) upto 3000 A $(m^2)^{-1}$. Experiments have been carried out using a planar electrolyte supported (ESC2) cell with a Ni-GDC anode under varying operating conditions of gas composition, temperatures and current densities. As the first step, the influence of the Ni current collector (mesh) on methane reforming has been shown. Kinetic trends have been established using both power law (PL) and Langmuir-Hinshelwood (LH) rate formulations for relatively low inlet steam concentrations (S/C around 1) and moderate current densities and a

first of its kind comparison has been presented to assess the suitability of using different rate expressions. This work is helpful to further verify rate and species distribution with future experiments and to design a more robust experimental approach incorporating the effects of metallic current collectors on MSR in Ni-based SOFCs. The presented data can be directly utilized for steady-state system and CFD model validation.

2. Experimental

2.1. Equipment and planar cell description

Fig. 1 shows a schematic of the experimental test bench used in the study. Dry gases (CH_4, H_2, O_2 and N_2) are fed to the SOFC from gas bottles using calibrated mass flow controllers (Bronkhorst EL-Flow Series) and pressure reducers. Steam is added to the dry inlet gas mix using a Bronkhorst controlled evaporator mixer (CEM) where the dry gases are mixed with controlled amount of water vapour. The anode inlet pipe is heat traced to maintain an inlet gas temperature of 120 °C. Hence all calculations including volume flow rates and S/C ratios have been carried out at this temperature. Simulated air (1200 mln min^{-1} N_2, 300 mln min^{-1} O_2) is used at the cathode inlet. The cathode off-gas is directly vented out. In order to calculate methane conversion (x) in the SOFC anode, the anode outlet gas was analyzed using a Agilent 490 micro GC. The micro GC consists of a Molsieve 5A column to measure the flow fraction of H_2, CH_4, CO and a PoraPLOT U column to measure the concentration of CO_2. The micro GC output concentrations were normalized to calculate the mole fractions of the various gases. To cool the anode outlet gas and prevent moisture entering the micro GC columns, a water filled bubbling condenser and a desiccant bottle (filled with silica gel) is used before the micro GC. A mass flow meter is then used to measure the total dry anode outlet flow. The system is operated at ambient (atmospheric) pressure. An electronic load unit (Kikusui, PLZ603W), supported with a compensation voltage unit (as power supply) is used for applying current to the cell. The load unit is operated in a constant current mode.

Commercial electrolyte supported cells (ESC2, manufactured by H.C Starck) were used to carry out the experimental investigation. The planar sqaure cell (9 × 9 cm active area) is placed on a square ceramic (alumina) block in a quadratic electrically heated (in presence of nitrogen) furnace which consists of a platinum current collector (or mesh) on the cathode side and a nickel mesh on the anode side. The cell consists of a 35 μm thick NiO-GDC (Ni-$Gd_{0.1}Ce_{0.9}O_{1.95}$) anode, 100 μm YSZ electrolyte and a 40 μm LSM ($La_{1-x}Sr_xMnO_{3-\delta}$) cathode. The anode consists of about 57% wt NiO. The planar cell is sealed gas tight in the ceramic block using Thermiculite (mica) seals both on the anode (0.3 mm thickness) and cathode (0.7 mm thickness) sides. Additional weight was added using a ceramic column on top of the block to ensure gas sealing.

2.2. Experimental methodology and current-voltage (I-V) characteristics

The NiO-GDC cell was reduced with a standard procedure at a temperature of 950 °C. A high reduction temperature has been used for an improved cell performance in consultation with SOFC manufacturers. The reduction procedure involved a gradual increase in the H_2 feed from a low H_2 concentration of about 2% (vol) to 100% over a period of 4 h. The cell was first tested for its performance with pure H_2. The area specific resistance (ASR) on pure H_2 at T_{cell} = 950 °C was about 0.79 Ω-cm^2.

The central aim of this study is to investigate MSR kinetics in operating Ni based SOFCs with lower steam concentrations (S/C around 1.0) at the anode inlet. In order to asses the effect of gas composition, 7 gas mixtures have been defined as shown in Table 2. The table gives the inlet gas composition in vol % and also the steam to carbon (S/C) ratio. A, B, C and D represent gas compositions with

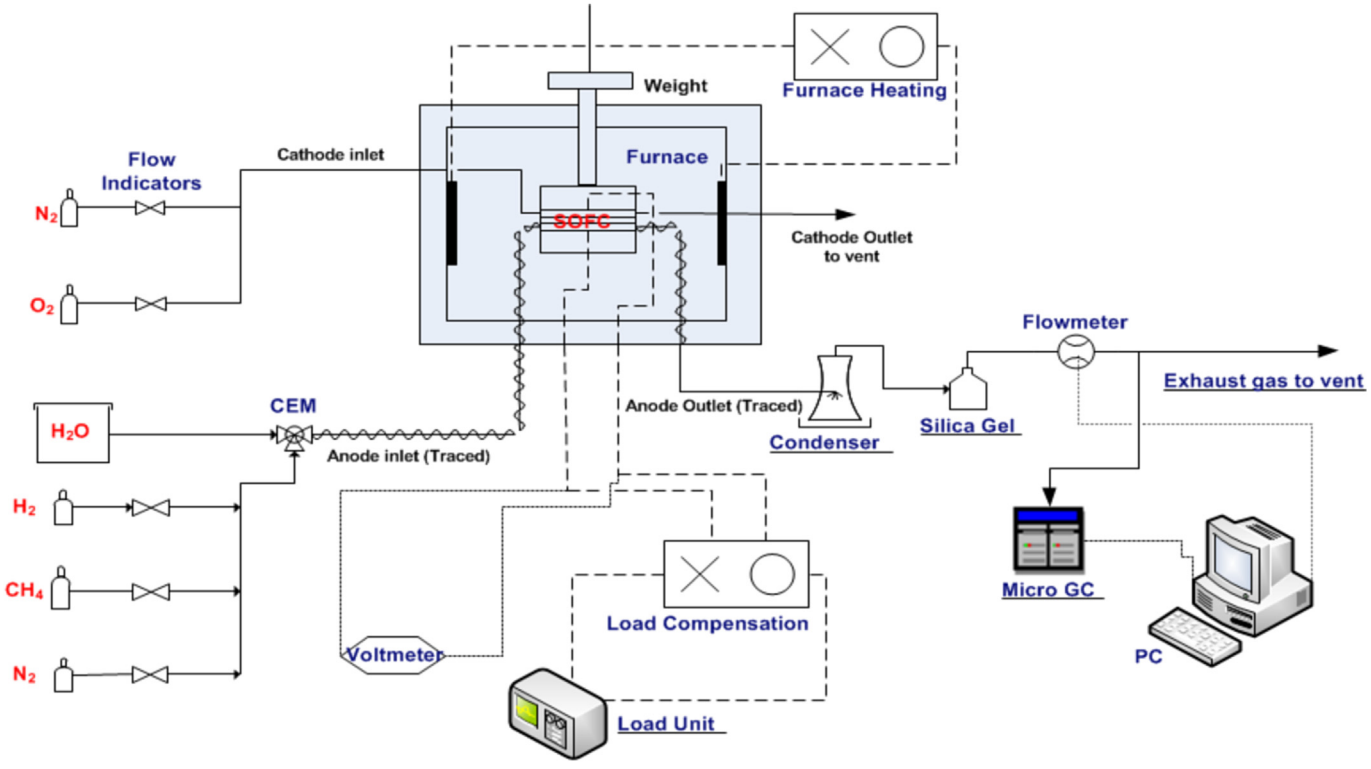

Fig. 1. Schematic of the experimental test bench.

increasing steam partial pressure while D, E, F and G represent gas compositions with increasing methane partial pressure. The N_2 flow is calculated to add up to a total inlet gas flow rate of 1200 mln min^{-1} (at T = 120 °C). The high total volumetric flow ensures flooded conditions and hence also results in low fuel utilizations. Minimal amount of H_2 was added to ensure a reducing environment in the anode. The experiments have been carried out at 3 different cell temperatures: 830 °C, 800 °C and 770 °C. Current imposed on the cell has been varied to obtain methane conversion data for current densities from 0 (open circuit conditions) to 3000 A $(m^2)^{-1}$. The calculated ASR was 1.61 Ω-cm^2 for composition A at T_{cell} = 830 °C.

Starting with the highest temperature, the anode inlet gas compositions were varied sequentially as listed in Table 2. For each inlet gas composition, the I-V characteristics and anode outlet gas composition have been obtained. The methane conversion (x) has been calculated based on the outlet gas composition (measured using Agilent 490 micro GC) and a carbon balance [4,52] using Eqn. (4):

$$x = \frac{y_{CO} + y_{CO_2}}{y_{CH4} + y_{CO} + y_{CO_2}} \tag{4}$$

where y_i denotes the mole fraction of gas species i. An important aspect to keep in mind to obtain y_i is to ensure a steady outlet gas composition. It was observed that a steady conversion is obtained after 8–9 h. Experimental measurements with all 7 gas compositions have been carried out ensuring steady flow.

3. Kinetic model and parameter estimation

A kinetic model which calculates kinetic parameters based on the experimental methane conversion (x) is essential to establish trends and further understand the reaction kinetics. This section describes the kinetic model developed in this study using the power law (PL) and Langmuir-Hinshelwood (LH) rate formulation.

3.1. Ideal plug flow reactor (IPFR) assumption

The MSR reaction rate can be mathematically expressed based on an ideal plug flow reactor (IPFR) assumption. This assumption can be justified due to the relatively small fuel channel dimensions, low gas velocities and low Reyolds number. Such a mathematical formulation is also based on an assumption that there is no pressure drop across the reactor and no catalyst decay. In reality, this is not true particularly with pressurized reactors; however in this experimental work, a significant deviation is not expected due to operation at ambient conditions. The MSR reaction rate (r_{CH_4}) across an elemental volume dV can be expressed as in Eqn. (5):

$$-r_{CH_4} = \frac{dF_{CH_4}}{dV} = \frac{d\left(F_{CH_4,0}(1-x)\right)}{dV} = -F_{CH_4,0}.\frac{dx}{dV} \tag{5}$$

where x is the methane conversion, F_{CH_4} is the methane molar flow rate (mol s^{-1}) and $F_{CH4,0}$ is the methane molar flow rate (mol s^{-1}) at the anode inlet. Integrating over the entire reactor volume V gives the rate equation as shown in Eqn. (6):

$$\frac{V}{F_{CH_4,0}} = \int_0^{x_{out}} \frac{dx}{-r_{CH_4}} \tag{6}$$

x_{out} represents the methane conversion at the anode outlet. The MSR reaction rate can also be expressed in terms of the species partial pressures thereby linking important kinetic parameters such as rate constant (k), reaction orders (α) and activation energy (E_a). The following sections describe the reaction rate equations using the Power law (PL) and Langmuir-Hinshelwood (LH) formulations.

Table 2
Anode inlet gas compositions for a total flow of 1200 mln min^{-1} at 120 °C.

vol %	CH_4	H_2O	H_2	N_2	S/C
A	33.00	36.90	3.30	26.80	1.13
B	33.00	39.30	3.30	24.40	1.20
C	33.00	41.80	3.30	21.90	1.28
D	33.00	44.30	3.30	19.40	1.35
E	36.00	44.30	3.30	16.40	1.24
F	38.90	44.30	3.30	13.50	1.15
G	41.80	44.30	3.30	10.60	1.07

3.2. Power law kinetic model

A simplistic approach to quantify MSR reaction kinetics is to formulate the rate equation assuming a single step reaction. With the law of mass action, this essentially leads to a power rate law type rate equation [53] as shown in Eqn. (7). k is the rate constant which is independant of species concentration, but dependant on other variables that influence the rate. It can be calculated using the Arrhenius equation (Eqn. (8)). k_0 is the pre-exponential factor, R is the universal gas constant and T is the operating temperature in K.

$$-r_{CH_4} = k \cdot p_{CH_4}^{\alpha_{CH_4}} \cdot p_{H_2O}^{\alpha_{H_2O}} \tag{7}$$

where

$$k = k_0 \cdot \exp\left(\frac{-E_a}{RT}\right) \tag{8}$$

Using Eqn. (6) and Eqn. (7), the rate constant k can be calculated per unit volume by evaluating the integral as shown in Eqn. (9):

$$k = F_{CH_4,0} \cdot \int_0^{x_{out}} \frac{dx}{p_{CH_4}^{\alpha_{CH_4}} \cdot p_{H_2O}^{\alpha_{H_2O}}} \tag{9}$$

The activation energy E_a can be obtained from the slope of the Arrhenius plot using Eqn. (10)(based on Eqn. (8)).

$$\ln(k) = \frac{-E_a}{R}.\frac{1}{T} + \ln(k_0) \tag{10}$$

In order to estimate kinetic parameters, the species partial pressures (p_i) need to be expressed as a function of the methane conversion (x). The methane partial pressure can be calculated as shown in Eqn. (11):

$$p_{CH_4} = f(1-x).P \tag{11}$$

The partial pressures of different species have been expressed in terms of the methane conversion x. However, in order to relate all flow rates to the inlet methane flow rate ($F_{CH4,0}$) and the total inlet molar flow rate ($F_{total,0}$), a factor f is defined as in Eqn. (12). Furthermore, the increase in the total number of moles due to the reforming reaction is also taken into account in the factor f. P is the total system pressure (atmospheric).

$$f = \left(\frac{F_{total,0}}{F_{CH_4,0}} + 2x\right)^{-1} \tag{12}$$

The hydrogen electrochemical reaction (Eqn. (3)) produces steam and this has to be considered while determining the partial

pressure for steam and hydrogen. For this reason a current to carbon ratio (CC) is defined as shown in Eqn. (13):

$$CC = \frac{I}{2F \cdot F_{CH_4,0} \cdot x_{out}} \tag{13}$$

where I the current in Amperes (A) and $F = 96485$ C mol^{-1} is the Faraday constant. The simultaneous occurence of the WGS reaction (Eqn. (2)) has also to be taken into account to calculate p_{CO} and p_{CO_2}. The progress of the WGS reaction can be expressed as $y = x \cdot x_{CO}$ y represents the amount of methane that is converted to carbon dioxide. The value of y can be calculated using the equilibrium constant ($K_{eq,wgs}$) for the reaction as shown in Eqn. (14):

$$K_{eq,wgs} = e^{-\frac{\Delta G^0_{wgs}}{RT}} = \frac{p_{CO_2} \cdot p_{H_2}}{p_{CO} \cdot p_{H_2O}} = \frac{y(HC + x(3 - CC) + y)}{(x - y)(SC - x(1 - CC) - y)} \tag{14}$$

In order to reduce computation time, $K_{eq,wgs}$ has been calculated based on a temperature fitted equation [54] as shown in Eqn. (15):

$$K_{eq,wgs} = e^{((4202.5/T) - 3.928)} \tag{15}$$

The steam and hydrogen partial pressures can then be calculated as shown in Eqn. (16) and Eqn. (17):

$$p_{H_2O} = f(SC - x(1 - CC) - y).P \tag{16}$$

$$p_{H_2} = f(HC + x(3 - CC) + y).P \tag{17}$$

SC and HC represent the steam to carbon and hydrogen to carbon ratio at anode inlet respectively. p_{CO} and p_{CO_2} can then be calculated as shown in Eqn. (18) and Eqn. (19):

$$p_{CO} = f(x - y).P \tag{18}$$

$$p_{CO_2} = fy.P \tag{19}$$

3.3. Langmuir-Hinshelwood (LH) kinetic model

Catalytic reactions like the MSR reaction in reality consist of a sequence of elementary steps. These multiple reaction steps involve the adsorption and desorption of reactants, products and intermediate species on the surface of the catalyst [55]. The classical theory of Langmuir helps in formulating a rate equation (called the Langmuir-Hinshelwood rate equation) taking into account adsorption/desorption on catalyst surfaces. The rate formulation is based on an assumption that all species are chemisorbed and accomodated on the surface before any reaction. Furthermore, a monolayer coverage is assumed. A general rate equation for reactions catalyzed by solids accounting for chemisorption can be written as a combination of 3 groups as shown in Eqn. (20) [53,56]:

$$r = \frac{(\text{kinetic factor})(\text{driving force})}{(\text{adsorption term})} \tag{20}$$

The driving force (df) gives information on the reaction equilibrium. For the MSR reaction, the driving force term (df) has been calculated for the various gas compositions and temperatures using Eqn. (21) assuming a surface reaction [53]:

$$\mathrm{d}f = 1 - \frac{p_{CO} \cdot {p_{H_2}}^3}{K_{eq,msr} \cdot p_{CH_4} \cdot p_{H_2O}} \tag{21}$$

$K_{eq,msr} = e^{-\frac{\Delta G^0_{msr}}{RT}}$ represents the equilibrium constant for the MSR reaction. In order to reduce computation time, $K_{eq,msr}$ has been calculated based on a temperature fitted equation [54] as shown in Eqn. (22):

$$K_{eq,msr} = e^{((-27070/T) + 30.032)} \tag{22}$$

The Langmuir-Hinshelwood rate equation including the kinetic factor(k) and the adsorption term (denominator) can be written as shown in Eqn. (23) [53,57]:

$$r_{CH_4} = k.p_{CH_4}.\frac{p^a_{H_2O}}{p^b_{H_2}}.\frac{\mathrm{df}}{\left(1 + K_{H_2O}\frac{p_{H_2O}}{p_{H_2}} + K_{CH_4}.p_{CH_4}\right)^2} \tag{23}$$

Xu et al. [15] have carried out comprehensive work on intrinsic MSR reaction kinetics with Ni-$MgAl_2O_4$ catalyst using LH rate expressions derived on the basis of a reaction scheme and rate determining step. They have formulated the rate expression on the hypothesis of dominant methane adsorption in line with many other literature studies [15,25,28]. The same presumption is also applied in this work in formulating Eqn. (23). Furthermore, since a detailed reaction mechanism and rate determining step has not been determined in this work, a general rate equation has been formulated with respect to the steam and hydrogen partial pressure. Hence exponents a and b for the steam and hydrogen partial pressures respectively, are optimally calculated in the kinetic model. A similar rate formulation has been previously utilized in the past to investigate MSR kinetics on a Ni-alumina catalyst [17]. The LH rate equation used in this work thus differs from that postulated in the work of Xu et al. [15] particularly with respect to the variable effect of steam and hydrogen partial pressure (p_{H2O},p_{H_2}) on the reaction rate. K_{CH_4} and K_{H2O} are the adsorption rate constants for methane and steam respectively. These adsorption rate constants can be estimated using an Arrhenius type equation as shown in Eqn. (24) and Eqn. (25):

$$K_{CH_4} = A_{CH_4} \cdot \exp\left(\frac{-\Delta H_{CH_4}}{RT}\right) \tag{24}$$

$$K_{H_2O} = A_{H_2O} \cdot \exp\left(\frac{-\Delta H_{H_2O}}{RT}\right) \tag{25}$$

where A_{CH_4} and A_{H2O} are the pre-exponential factors, ΔH_{CH_4} and ΔH_{H2O} are the adsorption enthalpies for methane and steam respectively. The adsorption enthalpies obtained by Xu et al. [15] ($\Delta H_{CH_4} = -38.28$ kJ mol^{-1}, $\Delta H_{H2O} = 88.68$ kJ mol^{-1}) have been utilized to calculate the adsorption rate constants. Table 3 shows the calculated adsorption parameters for the LH kinetic model. The validity of the methane adsorption constants has been evaluated on the basis of a few thermodynamic criteria/guideline [15,16,58] that are helpful to evaluate if the adsorption parameters are consistent and thermodynamically meaningful.

1. Adsorption is exothermic i,e $-\Delta H_{CH_4} > 0$. A negative methane adsorption enthalpy means that this rule is satisfied.
2. Decrease in entropy after adsorption. i,e $0 < -\Delta S_{CH_4} < S^0_{g,CH_4}$ or $\exp((-S^0_{g,CH_4})/R) < A_{CH_4} < 1$. S^0_{g,CH_4} represents the standard methane entropy which has a value of 186.1 J (mol K)$^{-1}$. Evaluation of $\exp((-S^0_{g,CH_4})/R)$ and Table 3 show that this rule is satisfied.
3. $\ln(A_{CH_4}) \leq (12.2 - 0.0014.\Delta H_{CH_4})/R$. Table 4 shows that this rule is also satisfied.
4. The absolute values of entropy change ($\Delta S_{CH_4} = -\ln(A_{CH_4}).R$) in this case are 41.61 J (mol K)$^{-1}$, 48.29 J (mol K)$^{-1}$, 46.11 J (mol K)$^{-1}$ for the three temperatures (830°C, 800 °C, 770 °C) respectively.

Table 3
Adsorption parameters for the LH kinetic model.

Temperature(°C)	K_{CH_4}	K_{H2O}	A_{CH_4}
830	0.4355	0.6415	0.0067
800	0.2173	0.2000	0.0003
770	0.3217	0.1301	0.0039

Table 4
Table showing that the calculated methane adsorption constants satisfy thermodynamic criteria 3.

Temperature(°C)	$\ln(A_{CH_4})$	$(12.2 - 0.0014.\Delta H_{CH_4})/R$
830	−5.00	1.47
800	−5.81	1.47
770	−5.54	1.47

Usually this value should be higher than 42 J (mol K)$^{-1}$ and thus this rule is also satisfied (except for the higher temperature).

Using Eqn. (6) and Eqn. (23), the rate constant k can be calculated per unit volume by evaluating the integral as shown in Eqn. (26):

$$k = F_{CH_4,0} \cdot \int_0^{x_{out}} \frac{dx}{p_{CH_4} \cdot \frac{p_{H_2O}^a}{p_{H_2}^b} \cdot \frac{df}{\left(1 + K_{CH_4} \cdot p_{CH_4} + K_{H_2O} \cdot \frac{p_{H_2O}}{p_{H_2}}\right)^2}} \quad (26)$$

Whether the rate formulation is of PL or LH type, calculation of the rate constant/kinetic factor k requires optimization, since k should be independant of the composition (as stated in section 3.2). For the power law case, the reaction orders α_{CH_4} and α_{H2O} are calculated for the minimum deviation in the value of k. The coefficient of variation (COV) (defined as the ratio of standard deviation to the mean) has been used as the parameter to be minimized. For the LH case, the exponents a and b for steam and hydrogen respectively are determined for the minimum COV in the value of k defined by Eqn. (26). Activation energy for the LH rate expression is calculated using the Arrhenius plot (Eqn. (10)). A MATLAB script (Appendix) has been developed to estimate the MSR reaction rate and kinetic parameters for both PL and LH rate formulations. Fig. 2 shows a flowsheet indicating the main logic of this script.

4. Results & discussion

A step-by-step investigation on intrinsic MSR kinetics has been carried out in this work to obtain reliable kinetic trends. As the first investigation, preliminary results have been presented for methane reforming on the Ni current collector. The following subsections describe the main results obtained using the PL and LH kinetic models and a comparison between MSR kinetics using both approaches. As the last subsection, results based on equilibrium calculations have been presented to investigate carbon deposition.

4.1. Methane reforming on Ni current collector (mesh)

In order to check the extent of the MSR reaction on the Ni-mesh and in the ceramic (alumina) block (in the absence of catalyst), a preliminary experimental test was carried out in this work. The test was carried out using an anode inlet gas composition of 33% vol CH_4, 37% H_2O and 30% N_2 and a total volumetric flow rate of 1200 mln min^{-1} for two cell temperatures of 900 °C and 800 °C.

Table 5 shows methane conversion obtained with and without (ceramic block and pipes) the Ni mesh. As shown, methane conversion with only the ceramic block (without a Ni-mesh) is rather low and negligible. For the case with the Ni-mesh, it is seen that methane conversion is still relatively high (10%) and not completely negligible, particularly at higher temperatures. The results reported in this work therefore indicate MSR kinetics on the combined SOFC anode and Ni-current collector (mesh).

The test carried out in this work was with a high (flooded condition) inlet volumetric flow rate. The total volumetric flow rate is an important parameter for this investigation as it directly affects the gas residence time (defined as the ratio of reactor volume and the total volumteric flow rate). For lower volumetric flow rates i,e higher residence time it is expected that methane conversion will be higher. This is an important consideration particularly for kinetic studies at high SOFC fuel utilizations. Additional experiments need to be carried out to verify this and establish more quantitatively the extent of methane conversion on the Ni-mesh; however this study clearly indicates that methane steam reforming on the metallic current collector may not be always negligible (except for low operating temperatures) and must be considered in SOFC kinetic studies. The following sections describe the results obtained using PL and LH formulations following with a brief section on carbon deposition.

4.2. Power law (PL) kinetics

Table 6 lists the experimental methane conversion (Eqn. (4)) at 3 different cell temperatures and 7 inlet gas compositions(see Table 2). The kinetic study using the PL formulation has been performed by analyzing various paramters like MSR reaction rate (at various operating temperatures, inlet gas compositions and current densities), reaction orders and the activation energy. Fig. 3a shows the MSR reaction rate distribution using the PL rate equation (Eqn. (7)) along the normalized channel length at various operating temperatures under open circuit (Ic0) conditions for composition D. The rate constant normalized reactor length has been calculated on the basis of methane conversion (x) and the maximum rate constant k. The MSR reaction rate increases with increasing operating temperatures, verifying previous studies in literature [7,17,26]. The plot further indicates a decreasing reaction rate along the fuel channel with p_{CH_4} highest at the inlet and decreasing along the channel (See Fig. 3d).

Fig. 3d shows a sharp increase in the hydrogen partial pressure (p_{H_2}) and a gradual increase in CO partial pressure (p_{CO}) along the reactor length, despite a decrease in the MSR reaction rate. Under open circuit conditions, bulk of the produced hydrogen (also produced with the WGS reaction) remains unconverted and furthermore the WGS reaction is assumed to reach equilibrium relatively fast. This results in an sharp increase in hydrogen concentration and a gradual increase in CO concentration along the reactor length. Fig. 3b shows the variation in the MSR reaction rate at $T_{cell} = 800$ °C with varying inlet gas compositions (p_{CH_4}, p_{H2O}) as listed in Table 2. The plot indicates a relatively strong positive influence of the methane partial pressure p_{CH_4} on the reaction rate (compositions D, E, F and G). This observation additionally verifies the similar trend reported in literature [7,17,22,23,27]. Furthermore it is also seen that the reaction rate is more strongly dependent on variation in p_{CH_4} (D, E, F, G) than the variation in p_{H2O} (A, B, C, D). Under open circuit conditions, steam has a mixed effect (positive influence when A and B are compared, negative influence when B, C and D are compared) on the MSR reaction rate. However it can be seen that the rate is fairly independant of the steam partial pressure (p_{H2O}) under the investigated range of operating conditions, confirming previous reports [22,23].

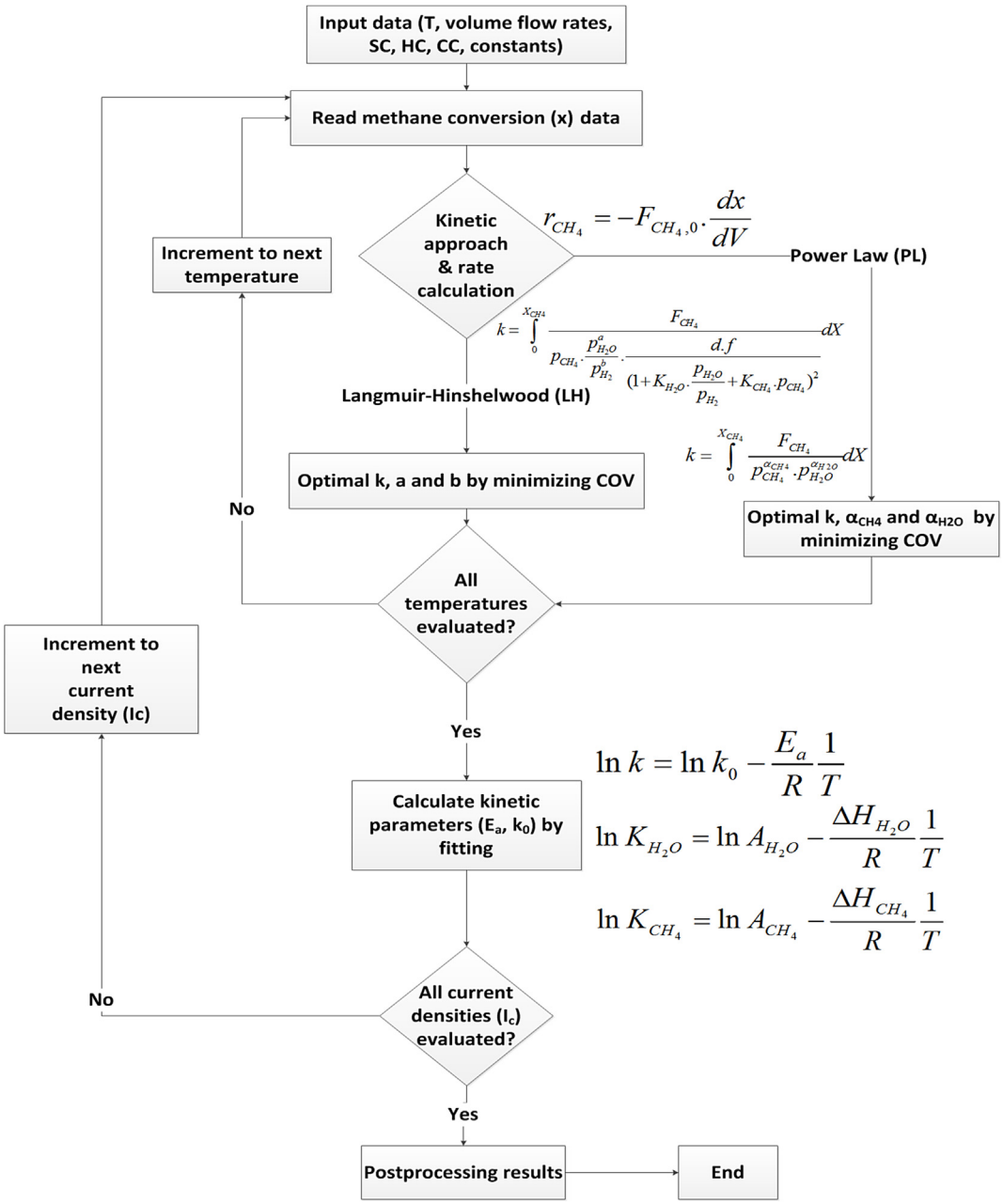

Fig. 2. Flowsheet indicating the approach for data fitting to obtain kinetic parameters.

Table 5
Methane conversion(x) on Ni current collector and ceramic block/pipes at 800 °C and 900 °C.

	Cell Temperature	
	900.00	800.00
Ni-Mesh	0.20	0.10
Ceramic block	0.02	0.01

4.2.1. Role of electrochemical oxidation

Under the influence of current, part of hydrogen produced via the MSR and WGS reaction is electrochemically oxidized to produce H_2O (see Eqn. (3)). Fig. 3c shows the variation in the MSR reaction rate along the channel length at open circuit (Ic0) and varying current densities of 500 A $(m^2)^{-1}$, 2000 A $(m^2)^{-1}$ and 3000 A $(m^2)^{-1}$. The plot indicates an increase in the MSR rate, although the increase is relatively marginal. The reaction rate is seen to increase slightly ($<2\%$) with increasing current densities. A slight increase in the outlet methane conversion (x) with increasing current densities as shown in Table 6 additionally verifies this trend.

Comparison between the species partial pressure at open circuit (Ic0) conditions and under load (at 3000 A $(m^2)^{-1}$) is also shown in Fig. 3d. The marginal increase in the MSR reaction rate is also reflected in the methane partial pressure distribution. A slight reduction in p_{CH_4} is observed with current. The plot also shows a significant decrease in p_{H_2} and a significant increase in p_{H2O} under load due to electrochemical oxidation. Fig. 3e shows the Arrhenius plots for various current densities and the linear fit (see Eqn. (10)) used to calculate the activation energy (E_a) and pre-exponential

Table 6
Experimental methane conversion.

Temperature (°C)	I_c (A $(m^2)^{-1}$)	Anode inlet composition						
		A	B	C	D	E	F	G
830	0	0.947	0.946	0.958	0.952	0.969	0.942	0.892
	500	0.977	0.955	0.956	0.955	0.980	0.965	0.934
	1000	0.986	0.961	0.961	0.959	0.985	0.975	0.969
	1500	0.990	0.964	0.963	0.961	0.988	0.980	0.978
	2000	0.992	0.967	0.966	0.963	0.990	0.983	0.985
	2500	0.994	0.969	0.967	0.965	0.991	0.985	0.987
	3000	0.995	0.972	0.970	0.968	0.992	0.987	0.990
800	0	0.903	0.930	0.937	0.929	0.895	0.887	0.825
	500	0.945	0.948	0.945	0.934	0.902	0.903	0.877
	1000	0.960	0.957	0.951	0.938	0.910	0.915	0.913
	1500	0.968	0.963	0.955	0.941	0.915	0.923	0.930
	2000	0.973	0.967	0.959	0.943	0.920	0.929	0.942
	2500	0.977	0.971	0.961	0.945	0.907	0.935	0.951
	3000	0.980	0.974	0.964	0.949	0.925	0.940	0.956
770	0	0.797	0.843	0.856	0.851	0.806	0.647	0.619
	500	0.856	0.869	0.863	0.861	0.814	0.655	0.636
	1000	0.902	0.887	0.871	0.868	0.824	0.658	0.658
	1500	0.914	0.897	0.877	0.873	0.833	0.678	0.684
	2000	0.928	0.905	0.884	0.878	0.840	0.687	0.708
	2500	0.937	0.914	0.891	0.886	0.850	0.700	0.725
	3000	0.943	0.920	0.900	0.893	0.859	0.707	0.743

factor (k_0). The plot indicates a decreasing rate constant k with increasing current densities in agreement with previous studies [7].

Fig. 3f shows the variation in the methane and steam reaction orders (α_{CH_4} and α_{H2O}) with varying current density. Under the influence of current, α_{CH_4} is positive and α_{H2O} is negative. A positive methane reaction order and a negative steam reaction order is also in agreement with previous findings in literature [7,30]. However, the reaction orders are seen to be dependant on the current density. With increasing current density, it is also seen that α_{CH_4} increases while α_{H2O} decreases. The strong decrease in α_{H2O} at higher current densities is thought to be due to the higher steam concentration in the anode due to electrochemical oxidation. A more rapid decrease in the steam reaction order compared to the methane reaction order with increasing current densities also indicates the significant difference in the reaction rate between MSR (Eqn. (1)) and H_2 electrochemical oxidation (Eqn. (3)). The local current density in an operating SOFC can vary significantly along the channel length. It is seen from this study that simplified global kinetic models using the PL rate expression yields a large set of reaction orders dependant on the local current density and hence it is concluded that such simplified approaches may not be suitable to develop global MSR kinetic models.

The next subsection describes the results obtained with the Langmuir-Hinshelwood (LH) kinetic model.

4.3. Langmuir-Hinshewood kinetics

In order to assess MSR kinetics with operating SOFCs, it is of utmost importance to first assess equilibrium conditions using the inlet gas compositions (Table 2). As aforementioned in section 3.3, the driving force (df) term (see Eqn. (21)) gives an indication of the reaction equilibrium. df should in principle be zero at conditions of equilibrium ensuring a zero reaction rate.

4.3.1. MSR reaction equilibrium

Table 7 lists the values for the equilibrium constant for the MSR ($K_{eq,msr}$) and WGS reaction ($K_{eq,wgs}$) which have been used to calculate df. Fig. 4a, Fig. 4b and c show the driving force distribution along the normalized reactor (channel) length for varying operating temperatures (at open circuit (Ic0) conditions and composition D), varying gas compositions(at T_{cell} = 800 °C and open circuit (Ic0) condition) and varying current densities (at T_{cell} = 800 °C and composition D) respectively. The plots indicate a high driving force near the inlet as the methane and steam partial pressure is highest near the inlet. The driving force decreases along the channel length due to the difference in species partial pressures (p_{CH_4}, p_{H2O}, p_{CO}, p_{H_2}), indicating that conditions near the anode outlet are closer to equilibrium. With a reduction in the cell temperature, df increases principally due to a lower $K_{eq,msr}$ and differences in the species partial pressures. Under the influence of current (Fig. 4c), it is seen that df increases along the channel when compared to open circuit (Ic0) conditions. This can be explained based on the fact that part of the produced hydrogen with the MSR reaction is consumed under the influence of current facilitating a higher driving force for the forward MSR reaction to occur.

4.3.2. Influence of temperature and inlet gas composition on MSR reaction rate

Fig. 5a shows the MSR reaction rate distribution along the normalized channel length at various operating temperatures for open circuit (Ic0) conditions and composition D. In addition, rate distributions are also shown for open circuit (Ic0) conditions and composition A (dashed curves). The plot indicates that MSR reaction rate increases with increasing operating temperatures. The reaction rate is maximum near the fuel inlet which is also in agreement with the PL prediction (see Fig. 3a). Fig. 5d indicates a subsequently decreasing methane partial pressure p_{CH_4} distribution along the reactor length. Fig. 5b shows the variation in the MSR reaction rate at T_{cell} = 800 °C and open circuit (Ic0) condition with varying inlet gas compositions. The plot clearly reconfirms the dominant role of inlet methane partial pressure p_{CH_4} (composition D, E, F and G) compared to the steam partial pressure.

4.3.3. Role of electrochemical oxidation

Fig. 5c shows the LH MSR reaction rate distribution along the normalized channel length at open circuit (Ic0) and current densities of 500 A $(m^2)^{-1}$ and 3000 A $(m^2)^{-1}$. The MSR reaction rate is seen to increase rapidly near the anode inlet (higher methane partial pressure) and reach a maximum near the inlet. Thereupon,

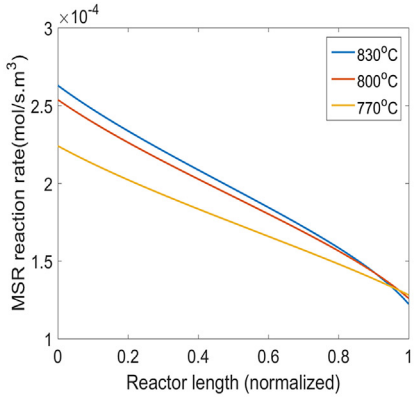

(a) MSR reaction rate at various operating temperatures for open circuit (Ic0) condition and composition D

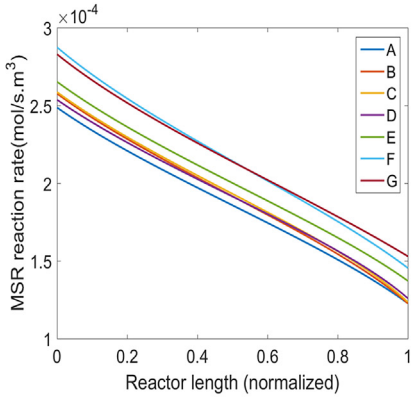

(b) MSR reaction rate at various anode inlet gas compositions for open circuit (Ic0) condition and T_{cell}=800^{o}C

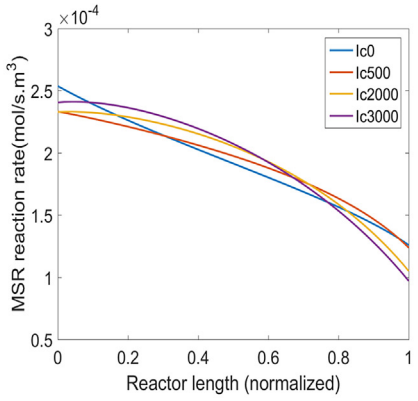

(c) MSR reaction rate at various current densities for T_{cell}=800^{o}C and composition D

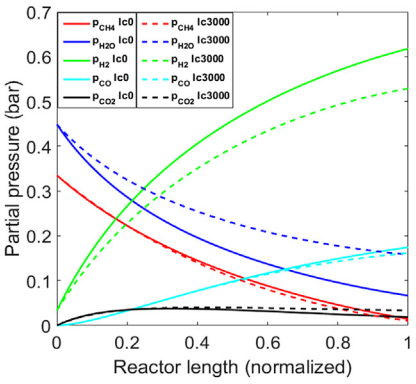

(d) Species partial pressure (bar) for open circuit (Ic0) and Ic=3000 A $(m^2)^{-1}$ and T_{cell}=800^{o}C and composition D

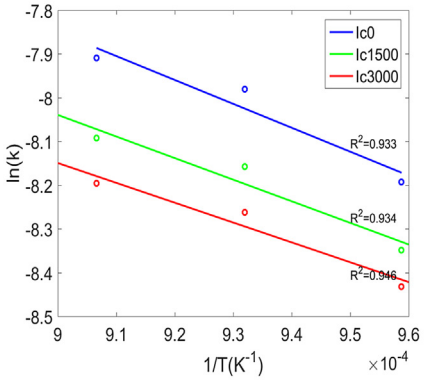

(e) Arrhenius plots with PL rate formulation at various current densities and T_{cell}=830^{o}C

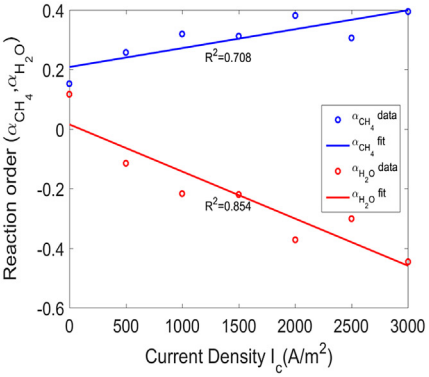

(f) Variation in α_{CH_4} and α_{H_2O} with current density

Fig. 3. Power law (PL) kinetic results.

Table 7
Equilibrium constants for the MSR and WGS reaction.

T_{cell} (°C)	$K_{eq,msr}$	$K_{eq,wgs}$
830	242.21	0.89
800	121.95	0.99
770	59.02	1.10

the reaction rate decreases along the reactor length. When the cell is operated on current, multiple processes occur within the anode which lead to a shift in the reaction rate maxima and a more gradual increase in the MSR reaction rate compared to open circuit (Ic0) conditions. Due to electrochemical hydrogen oxidation (Eqn. (3)), additional steam is produced increasing the partial pressure of steam, thereby lowering the MSR reaction rate [7,17]. Additionally there exists an effect of the cell temperature. Considering the combined interaction and different rates between the endothermic

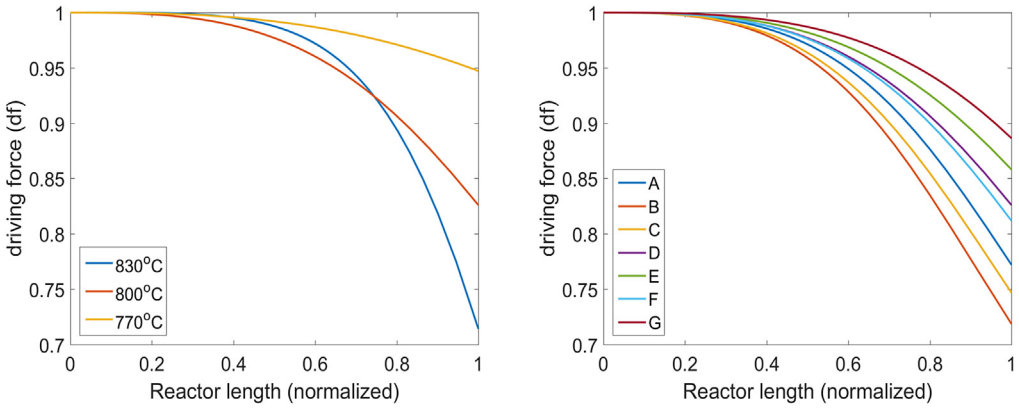

(a) Effect of cell temperature; for fixed composition D and open circuit (Ic0) condition

(b) Effect of inlet gas compositions; for fixed T_{cell}=800°C and open circuit (Ic0) condition

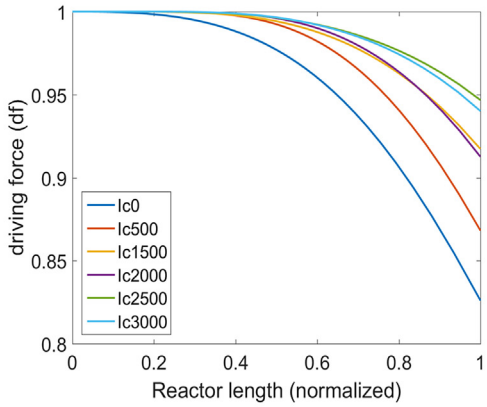

(c) Effect of current density; for fixed composition D and T_{cell}=800°C

Fig. 4. Driving force with the LH kinetic model.

MSR reaction (Eqn. (1)) and exothermic H_2 oxidation reaction (Eqn. (3)), the cell temperature is expected to vary under the influence of current. This temperature change has a direct influence on the MSR reaction rate. Thus, despite a net increase in MSR reaction rate under the influence of current, the local reaction rate is seen to increase more gradually under the influence of current. The effect of this is also visible in the species partial pressure distribution in Fig. 5d wherein the partial pressure of each specie varies more rapidly near the inlet under open circuit (Ic0) conditions.

Fig. 5c also shows a comparison between the MSR reaction rates between PL and LH approaches. The plot clearly indicates a significant difference in the reaction rate distribution with both approaches. The LH rate expression predicts a much higher reaction rate, particularly near the channel inlet and a lower rate near the outlet. The net reaction rate (obtained by calculating the area under the rate curve) for the PL and LH case at open circuit (Ic0), T_{cell} = 800 °C and composition D is 1.91e-04 mol (s m^3)$^{-1}$ and 1.90e-04 mol(s.m^3)$^{-1}$ respectively. This means that both the approaches predict the same net reaction rate but different rate distributions. Comparison between Figs. 3d and 5d also clearly shows that the species partial pressure change more rapidly in the LH case near the inlet compared to the PL case. The rate and species distribution are important considerations while predicting temperature gradients along the anode both with experiments and modeling. The fact that different kinetic approaches result in different local rate and species distribution along the channel length is an important aspect to be kept in mind to accurately predict temperature gradients in SOFC anodes.

Table 8 shows the calculated exponents *a* (for steam) and *b* (for hydrogen) for varying current densities. Negative values of *a* indicate a negative effect of steam partial pressure on the reaction rate. A similar observation was made also using the PL formulation (section 4.2.1) under the influence of current. However a highly non linear dependancy is observed in the steam and hydrogen partial pressures on the current density. This suggests a complex reaction mechanism and additionally a need for further mechanistic investigations on the basis of elementary reactions. As aforementioned, the local current density in an operating SOFC can vary significantly along the channel length. Ideally, using a predictive kinetic model reaction orders/exponents must be independant of the local current density. The LH global kinetic model in essence yields a large set of exponents *a* and *b* depending on the local current density. Hence rate expressions based on previously proposed expressions for Ni-catalysts [59] may not be directly suitable to predict global MSR kinetics for cermet anodes. Fig. 5e shows the Arrhenius plots for various current densities and the linear fit (see Eqn. (10)) used to calculate the activation energy (E_a) and pre-exponential factor (k_0). The plots reconfirm the trend of a decreasing rate constant *k* with increasing current densities as shown in the PL case (see section 4.2.1).

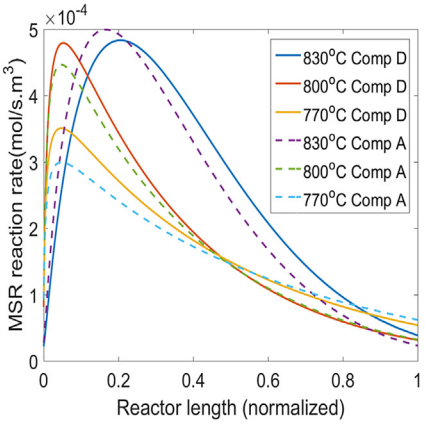

(a) MSR reaction rate at various operating temperatures for open circuit (Ic0) condition and composition D

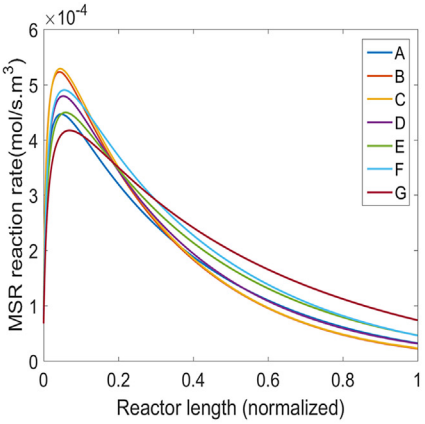

(b) MSR reaction rate at various anode inlet gas compositions for open circuit (Ic0) condition and T_{cell}=800°C

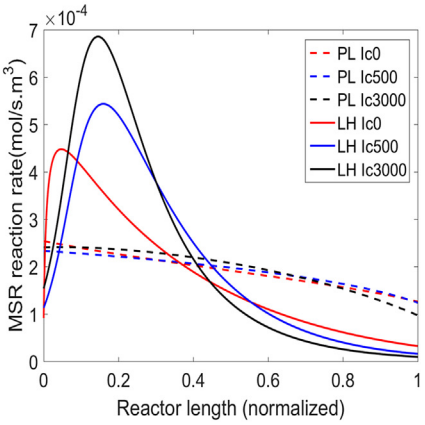

(c) MSR reaction rate at various current densities for T_{cell}=800°C and composition D

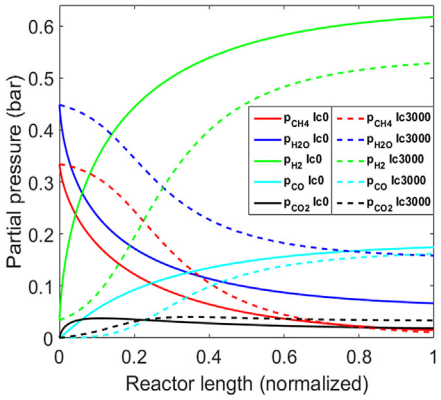

(d) Species partial pressure (bar) for open circuit (Ic0) and Ic=3000 A $(m^2)^{-1}$ and T_{cell}=800°C and composition D

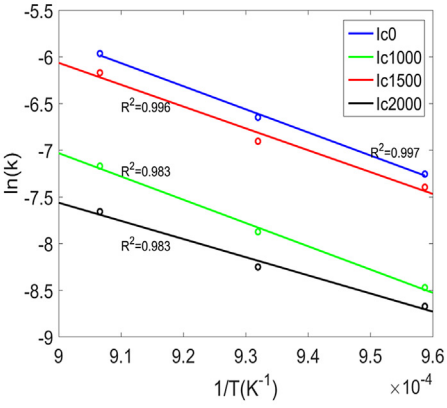

(e) LH Arrhenius plots at various current densities

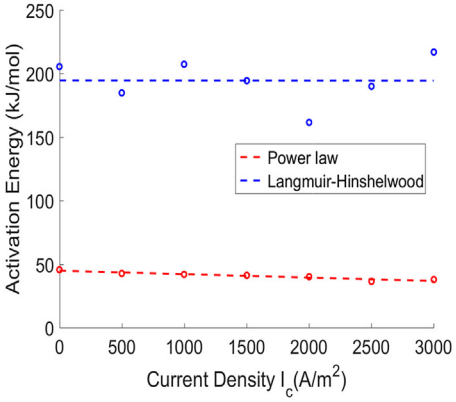

(f) Calculated activation energy (E_a)(kJ mol^{-1}) using PL and LH kinetic model for varying current densities

Fig. 5. Langmuir-Hinshelwood (LH) kinetic results.

Fig. 5f shows the variation in the activation energy (kJ mol^{-1}) with varying current densities both with the PL and LH rate expressions. The PL rate expression yields a lower activation energy compared to the LH rate expression. As the LH rate formulation also takes into account the adsorption/desorption enthalpies, the activation energy predicted with the LH rate is expected to be higher than the PL rate expression [55]. The values of activation energy predicted by both approaches are in agreement with previously reported values in literature [7,15,17,31]. Furthermore, it is seen that PL activation energy seems to be fairly constant with

Table 8
Calculated values of exponents a and b for varying current densities.

Ic (A $(m^2)^{-1}$)	a	b
0	0.007	1.210
500	−0.373	−0.033
1000	−0.610	1.339
1500	−0.555	0.271
2000	−1.117	0.583
2500	−0.596	0.014
3000	−0.843	−0.022

varying current densities. Results with the LH kinetic model indicate a larger difference in the activation energy compared to the PL, however this deviation is not very significant. A comparison between both approaches indicates that electrochemical oxidation (current) may not be causing a significant change in the activation energy. A detailed explanation on this can be obtained only on the basis of a more detailed investigation into the elementary MSR reaction chemistry.

This investigation hasn't been focussed to address in detail the reaction mechanism on Ni-GDC anodes. However the qualitative kinetic trends obtained in this work are helpful to deduce mechanistic details by comparison with elementary MSR kinetics on Ni-GDC anodes. A positive reaction order with respect to methane with both approaches is consistent with literature indicating methane adsorption as one of the rate controlling steps. This research, which clearly shows significant differences in the parametric (temperature, species) profiles along the channel length with PL and LH approaches can be directly used to assess the suitability of rate expressions by comparing with more detailed experiments. Extensive temperature probing and gas analysis along different points in the reactor could be used to obtain more accurate temperature and species distributions along the channel length. Research on such experimental activities is on-going in our research group and the results presented in this article are very helpful for comparison with such experiments and for further assessing the suitability of kinetic rate expressions.

It is well known that ceria plays an important role in the intrinsic MSR kinetics. Elementary MSR kinetics have been studied previously for Ni/YSZ anode supports by researchers [13,14]. They have proposed intrinsic micro-models with an extensive reaction mechanism with 42 elementary reactions involving 6 gas phase and 12 surface adsorbed species. Such models are very helpful and crucial for fundamental understanding and to obtain detailed parametric profiles across the fuel/oxidant channels. However, there hasn't been any research efforts yet to study elementary MSR kinetics on ceria based SOFC catalysts/anodes. In order to develop a more detailed kinetic model with a mechanistic outlook, additional experimental studies focussing on elementary reaction chemistry need to be carried out. Furthermore, based on elementary steps, energetics have to be evaluated using methods like UBI-QEP [60] and reactor network models. Based on fitting results obtained using experimental methane conversion and a comparison to the energetics obtained from elementary kinetics, indications could be obtained regarding the reaction mechanism and the rate determining step(s). Based on these rate determining step(s), global kinetic models could be developed which can be further readily implemented in dynamic cell/stack/system level models. This is out of scope for this work, however it is highly encouraged as a future research activity to improve our understanding on MSR intrinsic kinetics in Ni-ceria based operating SOFCs.

4.4. Carbon deposition

Carbon deposition is one of the most important operating challenge for SOFCs operated with hydrocarbon fuels. Presence of carbon containing species like CO, CO_2 and CH_4 on the anode side can lead to carbon formation. To check effects of the relatively low inlet S/C ratios used in this work, a brief analysis was carried using equilibrium calculations in Factsage (a commercial program to carry out multiphase equilibrium calculations) [61] and scanning electron microscopy with energy dispersive X-ray spectroscopy (SEM-EDX).

Thermodynamic equilibrium calculations are helpful to indicate theoretical limits for the operating paramters like temperature and S/C ratio. Fig. 6a shows a ternary diagram indicating the carbon (C), hydrogen (H) and oxygen(O) mole fractions at the anode inlet and anode outlet for two gas compositions (A and D) at $T_{cell} = 770\,^{\circ}C$. As it can be seen conditions at the anode inlet are closer to the gas-solid equilibrium line. Another important aspect to note is the right shift in the outlet conditions under the influence of current. As current is drawn more steam is produced due to the electrochemical hydrogen oxidation (Eqn. (3)) and this causes the O/C ratio to increase. Fig. 6b shows the oxygen to carbon ratio along the channel length at various current densities. Operating the cell at higher current densities causes the steam and oxygen concentration to increase along the channel. Furthermore, the O/C ratio decreases more rapidly under open circuit conditions compared to when operated under load.

Fig. 7 and Fig. 8 show the SEM image and the line plot from the EDX analysis respectively. Fig. 8 indicates the presence of a relatively low amount of carbon in the anode. This insignificant carbon count is attributed to cell manufacturing and deposited carbon species (intermediate) on the catalyst surface. No carbon deposition was observed visually on the anode surface after experimentation.

5. Conclusions

This article highlights the importance of carrying out experimental internal MSR global and intrinsic kinetic studies with complete Ni-ceria cermet anodes under the influence of current and for low S/C ratios. Further, it brings forward some limitations of using previously proposed rate equations to study global MSR kinetics on complete cermet anodes. A first of its kind comparative study has been performed using power law (PL) and Langmuir-Hinshelwood (LH) reaction rate expressions, to assess the effects of using different global kinetic formulations. The study further reports a trend analysis for various kinetic parameters such as reaction rate, reaction orders, activation energy and rate constants. Some important conclusions drawn from the work are listed below:

- Methane steam reforming on metallic (Ni/Pt) anode current collectors (mesh) may not always be negligible (particularly for operating temperatures above 800 °C) contrary to reports in literature.
- Both the PL and LH kinetic models predict exactly the same net MSR reaction rate, however there is a significant difference in the local rate and species distribution along the channel length. Despite both the approaches predicting a higher rate near the fuel inlet and lowest near the outlet, the LH approach predicts a much higher (peak) MSR reaction rate near the anode inlet compared to the PL approach leading to a different rate and species distribution.
- Both the global kinetic models show a large dependency of the reaction orders (PL) and exponents (LH) on the local current density, suggesting that simplified approaches (PL) and

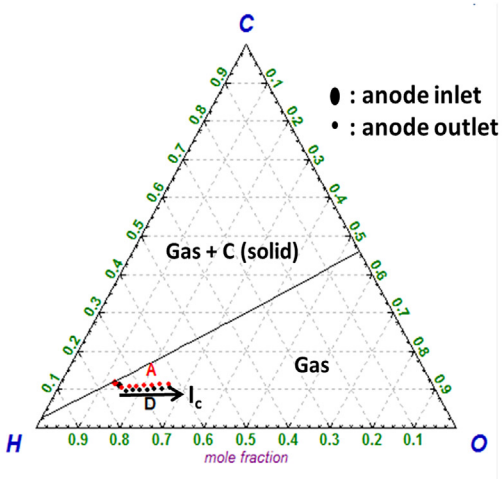

(a) Ternary diagram showing anode inlet and outlet conditions for composition A (red) and composition D (black) at T_{cell}=770°C with increasing current density (I_c)

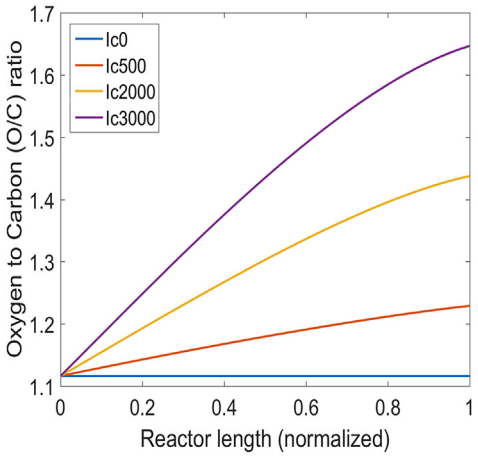

(b) Oxygen to Carbon (O/C) ratio along the reactor length at various current densities (I_c)

Fig. 6. Thermodynamic evaluation for carbon deposition.

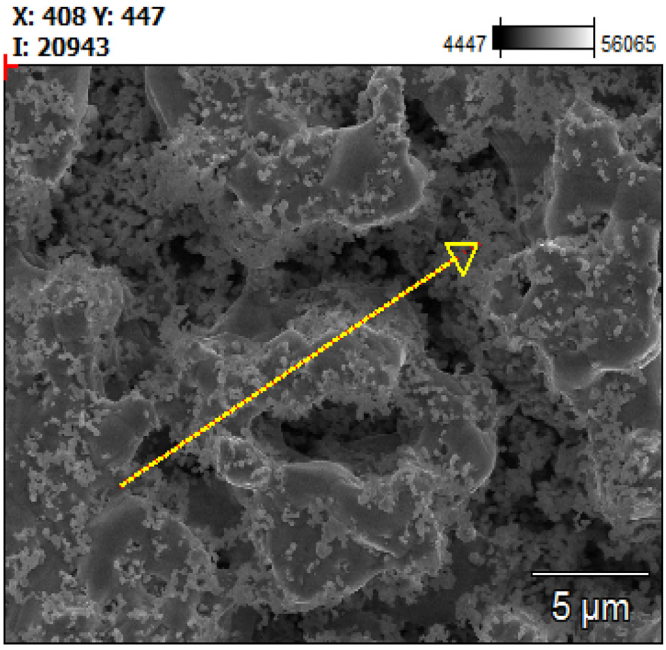

Fig. 7. SEM image of the anode cross section after experimentation.

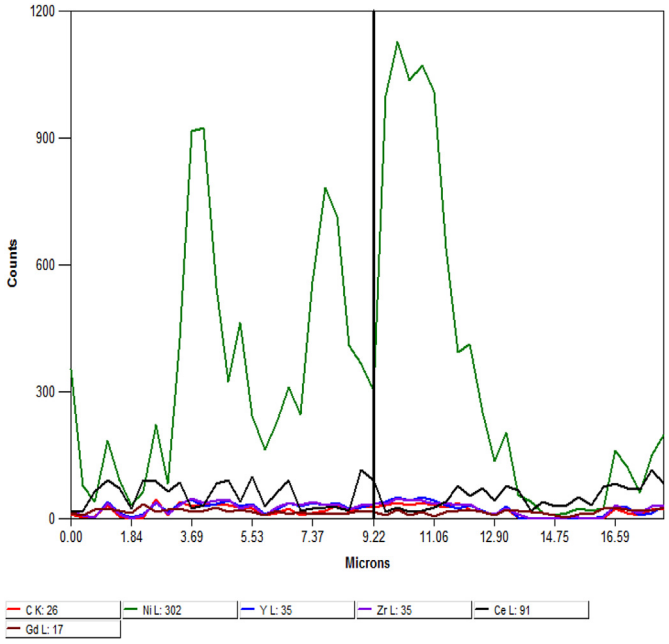

Fig. 8. Line scan EDX analysis for the Ni-GDC cell after experimentation.

previously proposed LH rate expressions for Ni catalytic beds may not be suitable to study MSR kinetics on complete cermet anodes under the influence of current.

- Both PL and LH kinetic approaches show that electrochemical oxidation (current) promotes methane conversion and the MSR reaction rate, however the effect of temperature is seen to be more dominant.
- The MSR reaction rate is a strong function of the inlet methane partial pressure.
- Electrochemical oxidation (current) seems to cause an insignificant change in the global MSR activation energy. However, further investigations on elementary reaction chemistry are required to verify this observation.
- The interaction between electrochemical oxidation (current) and the MSR reaction is highly complex suggesting the possibility of multiple rate determining steps depending of the operating condition; accurately predicting the intrinsic kinetics using a kinetic model requires the development of elementary reaction chemistry on Ni-ceria based anodes and further experimental investigations.
- No significant carbon deposition has been observed after the Ni-GDC cell was operated on methane with relatively low steam to carbon ratios of around 1.0–1.5.

The results obtained from this study provide insights into the influence of electrochemical reactions on MSR and show the

sensitivity in results due to different kinetic formulations. This work is helpful in formulating and comparing future experimental work and subsequently to assess the suitability of different rate expressions for complete Ni-ceria cermet anodes. Research on such experimental activities is on-going in our research group. The results can also be used for comparison with intrinsic MSR kinetic models for Ni-ceria based cells. Furthermore, data presented in this work can be used towards numerical (CFD) and system model development/validation.

Acknowledgements

The authors would like to thank David Hubertus (TU Munich, Germany) and Alessandro Beltrani (University of Bologna, Italy) for their significant help in laboratory measurements. Many thanks to Dr. Liyuan Fan for providing helpful discussions during the course of this work. The research was partly supported by funding from the CATO-2B project, the Dutch national project on carbon capture and storage (CCS).

References

[1] T.M. Gür, Comprehensive review of methane conversion in solid oxide fuel cells: prospects for efficient electricity generation from natural gas, Prog. Energy Combust. Sci. 54 (2016) 1–64. https://doi.org/10.1016/j.pecs.2015.10.004. http://www.sciencedirect.com/science/article/pii/S0360128515300496.

[2] R. O'Hayre, S.-W. Cha, W. Colella, F.B. Prinz, Chapter 1: Introduction, John Wiley & Sons, Inc, 2016, pp. 1–24, https://doi.org/10.1002/9781119191766.ch1. https://doi.org/10.1002/9781119191766.ch1.

[3] V.M. Janardhanan, V. Heuveline, O. Deutschmann, Performance analysis of a SOFC under direct internal reforming conditions, J. Power Sources 172 (1) (2007) 296–307. \{ACS\} San Francisco 2006Fuel and Cell Symposium. American Chemical Society National Meeting. San Francisco, \{CA\} Sept 10-14 2006, https://doi.org/10.1016/j.jpowsour.2007.07.008, http://www.sciencedirect.com/science/article/pii/S0378775307014759.

[4] G. Brus, Y. Komatsu, S. Kimijima, J. Szmyd, An analysis of biogas reforming process on Ni/YSZ and Ni/SDC catalysts, Int. J. Appl. Thermodyn. 15 (1) (2012) 43–51, https://doi.org/10.5541/ijot.315.

[5] C. Guerra, A. Lanzini, P. Leone, M. Santarelli, D. Beretta, Experimental study of dry reforming of biogas in a tubular anode-supported solid oxide fuel cell, Int. J. Hydrogen Energy 38 (25) (2013) 10559–10566. https://doi.org/10.1016/j.ijhydene.2013.06.074. http://www.sciencedirect.com/science/article/pii/S0360319913015449.

[6] C. Guerra, A. Lanzini, P. Leone, M. Santarelli, N.P. Brandon, Optimization of dry reforming of methane over Ni/YSZ anodes for solid oxide fuel cells, J. Power Sources 245 (2014) 154–163. https://doi.org/10.1016/j.jpowsour.2013.06.088. http://www.sciencedirect.com/science/article/pii/S0378775313010951.

[7] L. Fan, L. van Biert, A.T. Thattai, A. Verkooijen, P. Aravind, Study of methane steam reforming kinetics in operating solid oxide fuel cells: influence of current density, Int. J. Hydrogen Energy 40 (15) (2015) 5150–5159. https://doi.org/10.1016/j.ijhydene.2015.02.096. http://www.sciencedirect.com/science/article/pii/S0360319915004760.

[8] P. Aguiar, C. Adjiman, N. Brandon, Anode-supported intermediate temperature direct internal reforming solid oxide fuel cell. i: model-based steady-state performance, J. Power Sources 138 (1–2) (2004) 120–136. https://doi.org/10.1016/j.jpowsour.2004.06.040. http://www.sciencedirect.com/science/article/pii/S0378775304006950.

[9] Y. Matsuzaki, I. Yasuda, Electrochemical oxidation of H_2 and CO in a H_2-H_2O-CO-CO_2 system at the interface of a Ni-YSZ cermet electrode and YSZ electrolyte, J. Electrochem. Soc. 147 (5) (2000) 1630–1635, https://doi.org/10.1149/1.1393409. http://jes.ecsdl.org/content/147/5/1630.full.pdf+html. http://jes.ecsdl.org/content/147/5/1630.abstract.

[10] J.R. Rostrup-Nielsen, J. Sehested, J.K. Norskov, Hydrogen and Synthesis Gas by Steam- and CO2 Reforming, Vol. 47 of Advances in Catalysis, Academic Press, 2002, pp. 65–139. https://doi.org/10.1016/S0360-0564(02)47006-X. http://www.sciencedirect.com/science/article/pii/S036005640247006X.

[11] D. Mogensen, J.-D. Grunwaldt, P. Hendriksen, K. Dam-Johansen, J. Nielsen, Internal steam reforming in solid oxide fuel cells: status and opportunities of kinetic studies and their impact on modelling, J. Power Sources 196 (1) (2011) 25–38. https://doi.org/10.1016/j.jpowsour.2010.06.091. http://www.sciencedirect.com/science/article/pii/S0378775310010785.

[12] H. Patel, A. Tabish, F. Comelli, P. Aravind, Oxidation of h2, CO and syngas mixtures on ceria and nickel pattern anodes, Appl. Energy 154 (2015) 912–920. https://doi.org/10.1016/j.apenergy.2015.05.049. http://www.sciencedirect.com/science/article/pii/S0306261915006662.

[13] E.S. Hecht, G.K. Gupta, H. Zhu, A.M. Dean, R.J. Kee, L. Maier, O. Deutschmann, Methane reforming kinetics within a ni–ysz sofc anode support, Appl. Catal. A General 295 (1) (2005) 40–51, https://doi.org/10.1016/j.apcata.2005.08.003.

[14] H. Zhu, R.J. Kee, V.M. Janardhanan, O. Deutschmann, D.G. Goodwin, Modeling elementary heterogeneous chemistry and electrochemistry in solid-oxide fuel cells, J. Electrochem. Soc. 152 (12) (2005) A2427–A2440, https://doi.org/10.1149/1.2116607. http://jes.ecsdl.org/content/152/12/A2427.full.pdf+html. http://jes.ecsdl.org/content/152/12/A2427.abstract.

[15] J. Xu, G.F. Froment, Methane steam reforming, methanation and water-gas shift: I. intrinsic kinetics, AIChE J. 35 (1) (1989) 88–96.

[16] V. Arcotumapathy, F.S. Alenazey, R.L. Al-Otaibi, D.-V.N. Vo, F.M. Alotaibi, A.A. Adesina, Mechanistic investigation of methane steam reforming over ce-promoted Ni/SBA-15 catalyst, Appl. Petrochem. Res. 5 (4) (2015) 393–404, https://doi.org/10.1007/s13203-015-0121-2. https://doi.org/10.1007/s13203-015-0121-2.

[17] K. Hou, R. Hughes, The kinetics of methane steam reforming over a ni/α - al2o catalyst, Chem. Eng. J. 82 (2001) 311–328. https://doi.org/10.1016/S1385-8947(00)00367-3. http://www.sciencedirect.com/science/article/pii/S1385894700003673.

[18] A. Avetisov, J. Rostrup-Nielsen, V. Kuchaev, J.-H.B. Hansen, A. Zyskin, E. Shapatina, Steady-state kinetics and mechanism of methane reforming with steam and carbon dioxide over ni catalyst, J. Mol. Catal. A Chem. 315 (2) (2010) 155–162 in memory of M.I. Temkin, https://doi.org/10.1016/j.molcata.2009.06.013, http://www.sciencedirect.com/science/article/pii/S1381116909002866.

[19] W. Wang, C. Su, Y. Wu, R. Ran, Z. Shao, Progress in solid oxide fuel cells with nickel-based anodes operating on methane and related fuels, Chem. Rev. 113 (10) (2013) 8104–8151, https://doi.org/10.1021/cr300491e. https://doi.org/10.1021/cr300491e.

[20] K. Asai, Y. Nagayasu, K. Takane, S. Iwamoto, E. Yagasaki, K. ichi Ishii, M. Inoue, Mechanisms of methane decomposition over ni catalysts at high temperatures, J. Jpn. Petroleum Inst. 51 (1) (2008) 42–49, https://doi.org/10.1627/jpi.51.42.

[21] M. Andersson, H. Paradis, J. Yuan, B. Sunden, Review of catalyst materials and catalytic steam reforming reactions in sofc anodes, Int. J. Energy Res. 35 (15) (2011) 1340–1350, https://doi.org/10.1002/er.1875. https://doi.org/10.1002/er.1875.

[22] N. Nakagawa, H. Sagara, K. Kato, Catalytic activity of Ni-YSZ-CeO_2 anode for the steam reforming of methane in a direct internal-reforming solid oxide fuel cell, J. Power Sources 92 (1–2) (2001) 88–94. https://doi.org/10.1016/S0378-7753(00)00508-5. http://www.sciencedirect.com/science/article/pii/S0378775300005085.

[23] E. Achenbach, E. Riensche, Methane/steam reforming kinetics for solid oxide fuel cells, J. Power Sources 52 (2) (1994) 283–288. https://doi.org/10.1016/0378-7753(94)02146-5. http://www.sciencedirect.com/science/article/pii/0378775394021465.

[24] J. Parsons, S. Randall, Experimental determination of kinetic rate data for sofc anodes, in: SOFC-micromodelling IEA-SOFC Task Report, 1992, pp. 43–46.

[25] A.L. Lee, R. Zabransky, W. Huber, Internal reforming development for solid oxide fuel cells, Ind. Eng. Chem. Res. 29 (5) (1990) 766–773.

[26] S. Souentie, M. Athanasiou, D.K. Niakolas, A. Katsaounis, S.G. Neophytides, C.G. Vayenas, Mathematical modeling of ni/gdc and au–ni/gdc sofc anodes performance under internal methane steam reforming conditions, J. Catal. 306 (2013) 116–128, https://doi.org/10.1016/j.jcat.2013.06.015.

[27] A. Dicks, K. Pointon, A. Siddle, Intrinsic reaction kinetics of methane steam reforming on a nickel/zirconia anode, J. Power Sources 86 (12) (2000) 523–530. https://doi.org/10.1016/S0378-7753(99)00447-4. http://www.sciencedirect.com/science/article/pii/S0378775399004474.

[28] V.D. Belyaev, T.I. Politova, O.A. Mar'ina, V.A. Sobyanin, Internal steam reforming of methane over ni-based electrode in solid oxide fuel cells, Appl. Catal. A General 133 (1) (1995) 47–57, https://doi.org/10.1016/0926-860X(95)00184-0. http://ac.els-cdn.com/0926860X95001840/1-s2.0-0926860X95001840-main.pdf?_tid=bcbf116a-89e8-11e4-9f0d-00000aacb361&acdnat=1419259522_52e45688f1a8f792d69b4d-d5145e1cb4#page=1&zoom=auto,-186,453.

[29] S. Bebelis, A. Zeritis, C. Tiropani, S.G. Neophytides, Intrinsic kinetics of the internal steam reforming of ch4 over a ni-ysz-cermet catalyst-electrode, Ind. Eng. Chem. Res. 39 (12) (2000) 4920–4927, https://doi.org/10.1021/ie000350u. https://doi.org/10.1021/ie000350u.

[30] K. Ahmed, K. Foger, Kinetics of internal steam reforming of methane on Ni/YSZ-based anodes for solid oxide fuel cells, Catal. Today 63 (24) (2000) 479–487. https://doi.org/10.1016/S0920-5861(00)00494-6. http://www.sciencedirect.com/science/article/pii/S0920586100004946.

[31] H. Timmermann, D. Fouquet, A. Weber, E. Ivers-Tiffée, U. Hennings, R. Reimert, Internal reforming of methane at ni/ysz and ni/cgo sofc cermet anodes, Fuel Cells 6 (3–4) (2006) 307–313, https://doi.org/10.1002/fuce.200600002.

[32] O.A. Marina, C. Bagger, S. Primdahl, M. Mogensen, A solid oxide fuel cell with a gadolinia-doped ceria anode: preparation and performance, Solid State Ionics 123 (14) (1999) 199–208. https://doi.org/10.1016/S0167-2738(99)00111-3. http://www.sciencedirect.com/science/article/pii/S0167273899001113.

[33] H.C. Patel, T. Woudstra, P.V. Aravind, Thermodynamic analysis of solid oxide fuel cell gas turbine systems operating with various biofuels, Fuel Cells 12 (6) (2012) 1115–1128, https://doi.org/10.1002/fuce.201200062. https://doi.org/10.1002/fuce.201200062.

[34] J. Hanna, W.Y. Lee, Y. Shi, A.F. Ghoniem, Fundamentals of electro- and thermochemistry in the anode of solid-oxide fuel cells with hydrocarbon and syngas fuels, Prog. Energy Combust. Sci. 40 (2014) 74–111.

[35] E.P. Murray, T. Tsai, S.A. Barnett, A direct-methane fuel cell with a ceria-based anode, Nature 400 (6745) (1999) 649–651. https://doi.org/10.1038/23220.
[36] W.C. Chueh, Y. Hao, W. Jung, S.M. Haile, High electrochemical activity of the oxide phase in model ceria-pt and ceria-ni composite anodes, Nat. Mater 11 (2) (2012) 155–161. https://doi.org/10.1038/nmat3184.
[37] W. Wang, S.P. Jiang, A.I.Y. Tok, L. Luo, Gdc-impregnated ni anodes for direct utilization of methane in solid oxide fuel cells, J. Power Sources 159 (1) (2006) 68–72 special issue including selected papers from the 3rd International Conference on Materials for Advanced Technologies (ICMAT 2005, Singapore, Malaysia) and the Summer School on Synthesis of Nanostructured Materials for Polymer Batteries (Augustów, Poland) together with regular papers, https://doi.org/10.1016/j.jpowsour.2006.04.051, http://www.sciencedirect.com/science/article/pii/S0378775306006896.
[38] S.P. Jiang, S. Zhang, Y.D. Zhen, A.P. Koh, Performance of GDC-impregnated ni anodes of SOFCs, Electrochem. Solid-State Lett. 7 (9) (2004) A282–A285, https://doi.org/10.1149/1.1783112. http://esl.ecsdl.org/content/7/9/A282.full.pdf+html. http://esl.ecsdl.org/content/7/9/A282.abstract.
[39] B. Mosqueda, J. Toyir, A. Kaddouri, P. Gelin, Steam reforming of methane under water deficient conditions over gadolinium-doped ceria, Appl. Catal. B Environ. 88 (2009) 361–367. https://doi.org/10.1016/j.apcatb.2008.11.003. http://www.sciencedirect.com/science/article/pii/S0926337308004116.
[40] P.V. Aravind, J.P. Ouweltjes, N. Woudstra, G. Rietveld, Impact of biomass-derived contaminants on SOFCs with ni/gadolinia-doped ceria anodes, Electrochem. Solid-State Lett. 11 (2) (2008) B24–B28, https://doi.org/10.1149/1.2820452. http://esl.ecsdl.org/content/11/2/B24.full.pdf+html. http://esl.ecsdl.org/content/11/2/B24.abstract.
[41] H. Paradis, M. Andersson, J. Yuan, B. Sunden, CFD Modeling: different kinetic approaches for internal reforming reactions in an anode-supported SOFC, J. Fuel Cell Sci. Technol. 8 (3) (2011), https://doi.org/10.1115/1.4002906, 031014–031014–8, https://doi.org/10.1115/1.4002906.
[42] K. Wang, D. Hissel, M. Pera, N. Steiner, D. Marra, M. Sorrentino, C. Pianese, M. Monteverde, P. Cardone, J. Saarinen, A review on solid oxide fuel cell models, Int. J. Hydrogen Energy 36 (12) (2011) 7212–7228. https://doi.org/10.1016/j.ijhydene.2011.03.051. http://www.sciencedirect.com/science/article/pii/S0360319911006410.
[43] M. Andersson, J. Yuan, B. Sunden, Review on modeling development for multiscale chemical reactions coupled transport phenomena in solid oxide fuel cells, Appl. Energy 87 (5) (2010) 1461–1476. https://doi.org/10.1016/j.apenergy.2009.11.013. http://www.sciencedirect.com/science/article/pii/S0306261909005005.
[44] S. Kakac, A. Pramuanjaroenkij, X.Y. Zhou, A review of numerical modeling of solid oxide fuel cells, Int. J. Hydrogen Energy 32 (7) (2007) 761–786 fuel Cells, https://doi.org/10.1016/j.ijhydene.2006.11.028, http://www.sciencedirect.com/science/article/pii/S0360319906005726.
[45] A. Amiri, S. Tang, P. Vijay, M.O. Tade, Planar solid oxide fuel cell modeling and optimization targeting the stack's temperature gradient minimization, Ind. Eng. Chem. Res. 55 (27) (2016) 7446–7455, https://doi.org/10.1021/acs.iecr.6b01611. https://doi.org/10.1021/acs.iecr.6b01611. https://doi.org/10.1021/acs.iecr.6b01611.
[46] P. Hofmann, K. Panopoulos, L. Fryda, E. Kakaras, Comparison between two methane reforming models applied to a quasi-two-dimensional planar solid oxide fuel cell model, Energy 34 (12) (2009) 2151–2157 eCOS 2007, https://doi.org/10.1016/j.energy.2008.09.015, http://www.sciencedirect.com/science/article/pii/S0360544208002399.
[47] J. Li, G.-Y. Cao, X.-J. Zhu, H.-Y. Tu, Two-dimensional dynamic simulation of a direct internal reforming solid oxide fuel cell, J. Power Sources 171 (2) (2007) 585–600. https://doi.org/10.1016/j.jpowsour.2007.07.029. http://www.sciencedirect.com/science/article/pii/S0378775307014966.
[48] P. Aguiar, C. Adjiman, N. Brandon, Anode-supported intermediate-temperature direct internal reforming solid oxide fuel cell, J. Power Sources 147 (1) (2005) 136–147. https://doi.org/10.1016/j.jpowsour.2005.01.017. http://www.sciencedirect.com/science/article/pii/S0378775305001473.
[49] H. Xi, J. Sun, V. Tsourapas, A control oriented low order dynamic model for planar sofc using minimum gibbs free energy method, J. Power Sources 165 (1) (2007) 253–266. https://doi.org/10.1016/j.jpowsour.2006.12.009. http://www.sciencedirect.com/science/article/pii/S0378775306025201.
[50] N. Chatrattanawet, S. Skogestad, A. Arpornwichanop, Control structure design and dynamic modeling for a solid oxide fuel cell with direct internal reforming of methane, Chem. Eng. Res. Des. 98 (2015) 202–211. https://doi.org/10.1016/j.cherd.2015.04.029. http://www.sciencedirect.com/science/article/pii/S0263876215001434.
[51] K. Ahmed, K. Foger, Analysis of equilibrium and kinetic models of internal reforming on solid oxide fuel cell anodes: effect on voltage, current and temperature distribution, J. Power Sources 343 (2017) 83–93. https://doi.org/10.1016/j.jpowsour.2017.01.039. http://www.sciencedirect.com/science/article/pii/S0378775317300393.
[52] N. Itoh, T. Yamamoto, T. Sato, W. Yu, T. Ohmori, Kinetic analysis on low-temperature steam reforming of methane using a ruthenium supported catalyst, J. Jpn. Inst. Energy 85 (4) (2006) 307–313, https://doi.org/10.3775/jie.85.307.
[53] G.F. Froment, K.B. Bischoff, J.D. Wilde, Chemical Reactor Analysis and Design 3rd Edition, John Wiley & Sons, 2011.
[54] S. Elnashaie, A. Adris, A. Al-Ubaid, M. Soliman, On the non-monotonic behaviour of methane-steam reforming kinetics, Chem. Eng. Sci. 45 (2) (1990) 491–501. https://doi.org/10.1016/0009-2509(90)87036-R. http://www.sciencedirect.com/science/article/pii/000925099087036R.
[55] I. Chorkendorff, J.W. Niemantsverdriet, Concepts of Modern Catalysis and Kinetics, Wiley-VCH Verlag GmbH & Co. KGaA, 2005, pp. 23–78, https://doi.org/10.1002/3527602658.ch2. Ch. Kinetics, https://doi.org/10.1002/3527602658.ch2.
[56] K.H. Yang, O.A. Hougen, Determination of mechanism of catalyzed gaseous reactions, Chem. Eng. Prog. 46 (1950) 146.
[57] J. Xu, G.F. Froment, Methane steam reforming, methanation and water-gas shift: I. intrinsic kinetics, AIChE J. 35 (1) (1989) 88–96, https://doi.org/10.1002/aic.690350109. https://doi.org/10.1002/aic.690350109.
[58] M.A. Vannice, Kinetic Data Analysis and Evaluation of Model Parameters for Uniform (Ideal) Surfaces, Springer, US, Boston, MA, 2005, pp. 106–140, https://doi.org/10.1007/978-0-387-25972-7_6. https://doi.org/10.1007/978-0-387-25972-7_6.
[59] J. Xu, G. F. Froment, Methane steam reforming, methanation and water-gas shift: I. intrinsic kinetics, AIChE J.. URL http://onlinelibrary.wiley.com/store/10.1002/aic.690350109/asset/690350109_ftp.pdf?v=1&t=i1ujqtke&s=6da090625f5b7f676ec93e90ca19741c0fd50e09.
[60] E. Shustorovich, H. Sellers, The UBI-QEP method: a practical theoretical approach to understanding chemistry on transition metal surfaces, Surf. Sci. Rep. 31 (1) (1998) 1–119. https://doi.org/10.1016/S0167-5729(97)00016-2. http://www.sciencedirect.com/science/article/pii/S0167572997000162.
[61] C.W. Bale, P. Chartrand, S.A. Degterov, G. Eriksson, K. Hack, R.B. Mahfoud, J. Melancon, A.D. Pelton, S. Petersen, Factsage 6.4. http://www.factsage.com/.